Graphene Synthesis on Electrodeposited Substrates and Its Integration in MEMS for Sensor Applications

M. Tocchio[a], S. Ieffa[a], R. Bernasconi[a], L. Magagnin[a]*, L. Nobili[a], C. Carraro[b], R. Maboudian[b]

[a] Dipartimento di Chimica, Materiali e Ingegneria Chimica G. Natta, Politecnico di Milano, Via Mancinelli 7, 20131, Milan, Italy

[b] Department of Chemistry and Biomolecular Engineering, University of California, Berkeley, California 94720, USA

*Corresponding author: luca.magagnin@polimi.it

The synthesis of graphene on dealloyed NiCu is reported. The existence, thickness, and quality of the graphene films are discussed based on their Raman spectra. The growth of graphene on dealloyed NiCu is affected by the amount of copper in the alloy: a transition from graphitic to graphenic layers is observed with increasing copper content. Transfer procedures devised to integrate the graphene layers into functional devices are presented. The experimental results suggest the possibility of using this simple approach to develop new transducing materials integrated with silicon microdevices for sensing applications.

Introduction

Graphene has become a promising material for many different applications, such as nanoelectronic devices (1,2), physical, chemical, and biochemical sensors (3), transparent conductive films, clean energy scavenging and storage devices (4,5), and nanocomposite formulations. This great variety of possibilities is facilitated by the exceptional charge transport, optical, and mechanical properties of the material (6). Sensing applications using graphene sheets as transducers have attracted a surge of research activities in recent years, especially for gas sensing platforms and electrochemical sensing, because of the high electrical conductivity and high surface area of grapheme (3,7,8). The most intriguing feature of graphene based sensors is that proper functionalization of graphene enables enhanced selectivity and improved performance. Moreover, by combining graphene electronic and mechanical properties, monolithic sensors with superior sensitivity can be developed. Despite the significant amount of work on graphene electronic devices such as the field effect transistor, its use in sensors, actuators or micro and nano-electromechanical systems (MEMS/NEMS) in general is relatively less explored. In this work, the synthesis of graphene by benzene decomposition (9-12) at different temperatures onto free standing electrodeposited substrates is investigated, allowing to study the effects of electrochemically produced substrates on graphene quality. The growth of good quality graphene layers is discussed in terms of the role played by grain boundaries and by diffusion at the grain boundaries. Substrates present tunable porosity

obtained by dealloying the electrodeposited NiCu precursor. The specific area of the structure obtained is therefore greatly enhanced, which is a desirable feature in sensing application. An additional attractive feature demonstrated in this work is the possibility to decorate graphene layers with noble metals nanoparticles.

Materials and methods

The electrochemical experiments were developed in a conventional three-electrode cell using a Solartron Analytical Modulab equipment and a Modulab ECS software. The working electrode was an ultra-smooth 316L stainless steel plate, while counter and reference electrodes were a nickel plate and a SCE respectively. Potentiostatic deposition was selected in order to achieve a constant and uniform composition throughout the deposits (13). The chemicals used for the aqueous solution preparation were 710.42 g/l $Ni(H_2NSO_3)_2 \oplus 4H_2O$, 7.96 g/l $CuCO_3$, 4.33 g/l CH_3COOH, 52.94 g/l $Na_3C_6H_5O_7 \oplus 2H_2O$ and 0.5 g/l saccharine. All the chemicals were purchased from Sigma Aldrich and used as received. High citrate concentration was chosen to delay the copper reduction process onset towards more negative potential. Saccharine was selected to reduce the tensile stress into the deposits and to guarantee the planarity of the detached free-standing NiCu alloy films (13). The experiments were developed at room temperature under stirring condition (ω = 300 rpm), while the solution pH was kept between 4 and 5, being the best range for the electrodeposition from the NiCu system (13). Composition and thickness were determined by a Fisherscope X-Ray XAN instrument. Cyclic voltammetries were acquire using the Modulab equipment. After every electrodeposition, the detachment of the deposited films form the ultra-smooth stainless steel plate was obtained simply using a cutter and, subsequently, the free-standing foils were rinsed in abundant DI water and then dried with a nitrogen flux. The annealing of the samples was performed in a Carbolite tubular oven. Graphene growth was obtained through low temperature CVD using liquid benzene as carbon source (12). 0.8 μL of liquid benzene were poured in a ceramic container placed at the beginning of the quartz tube of the CVD reactor and kept at room temperature for the whole process. Then, liquid benzene together with 65 sccm of Ar were let flow for five minutes at room temperature in order to saturate the quartz tube with the benzene molecules. Subsequently, the reactor was brought at the desired temperature and four minutes was the growth time. Finally, a cooling step at 20 °C/min was carried out. The Raman graphs were acquired by mean of a Horiba Jobin Yvon Labram spectrometer, with excitation provided by a HeNe laser (633 nm). For SEM characterization a Zeiss EVO 50 EP equipped with two version of the supporting software was used. Optical microscopy was performed using a Laica DMLM direct illumination microscope.

Results

The fabrication of porous Ni substrates was obtained through a two-step electrochemical process. Initially, foils of NiCu alloy with different compositions were electroformed on a ultra-smooth stainless steel plate. Then, free-standing nanoporous Ni films were obtained by selective electrochemical dealloying in the NiCu system. The operative conditions, as applied voltage and solution pH, for both the electrochemical processes were found to have a great influence on the morphology and composition of the final samples. Since the final purpose was to produce free-standing nanoporous Ni foils via electrochemical

etching of copper from the electrodeposited NiCu system, starting deposits with a high nickel percentage were desired. This is due to the fact that during the etching phase, the Ni structural stability is heavily undermined; therefore, compact, homogeneous and Ni-rich films were required.
Cyclic voltammetry (CV) was used to investigate the electrochemical behavior of the electrolyte and to estimate the potentials suitable for electroforming (fig. 1).

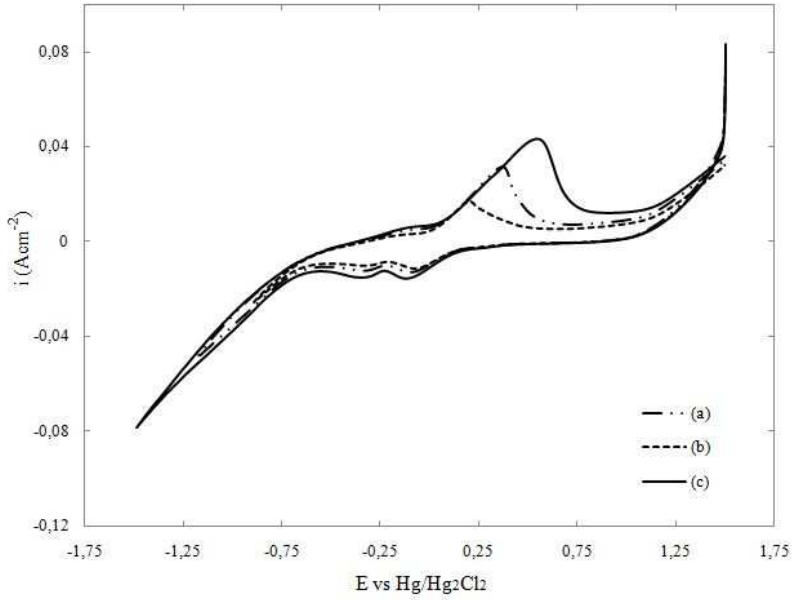

Figure 1. Cyclic voltammograms of 0.4 M Ni(II) + 0.02 M Cu(II) + 0.18 M $C_6H_5Na_3O_7 \cdot 2H_2O$ at scan rate 50 mVs^{-1}, no stirring and different cathodic limits: curve (a) -1.2 V, curve (b) -0.9 V, curve (c) -1.5 V.

As shown in Fig.1, CV measurements proved that the difference between the copper (II) and nickel (II) reduction peaks was lower compared to the theoretical difference between the standard reduction potentials of the two metals. In particular the Cu^0 reduction peak was found near -0.15 V, while the Ni^0 peak was detected at -0.35 V. As a consequence, since at more negative potential than E_{eq}^{Ni} copper deposition is diffusion-limited, whereas nickel deposition rate increases with decreasing potential (13, 14), it has been decided to work at quite negative potential, namely in a range between -0.8 V and -1.3 V. Effects of the applied potential and solution pH on the final composition of the electrodeposited alloy films are displayed in Fig.2.

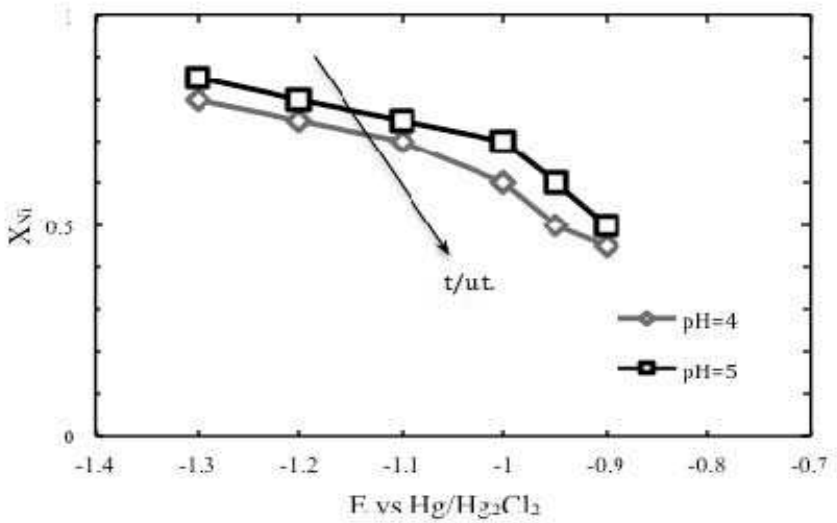

Figure 2. Mole fraction of Ni vs. deposition potential of the electrodeposited Ni_xCu_{1-x} films. The arrow indicates the film thickness trend per unit time.

Higher Ni percentages were obtained at more negative potentials and with a solution pH equal to 5 (fig. 2). In Tab. 1 the characteristics of the obtained alloy films as a function of solution pH and applied potential are shown. Moreover, the electroformed films were metallic grey, compact, homogeneous and brighter with higher Ni percentages. Furthermore, deposits obtained at fixed electrodeposition conditions, but at different deposition time showed the same composition.

Table I. Composition and thickness of electrodeposited Ni-Cu alloy films prepared potentiostatically under stirred conditions (ω = 300 rpm) over ultra-smooth stainless steel plate for different applied potentials.

pH	E(V)	Alloy composition (% Cu)	Deposit thickness (μm)
4	-1.2	25	15
4	-1.1	30	11
4	-1.0	40	9
5	-1.2	20	18
5	-1.1	25	14
5	-1.0	30	9

The obtained deposits were then separated from the substrate. Since electrodeposition induces internal stresses into the deposits, a thermal treatment at 400 °C for 1 hour and under nitrogen atmosphere was carried out on each NiCu strip in order to relief those internal stresses. This step was necessary to ensure the mechanical stability and structural integrity of the free-standing films during the following electrochemical dealloying phase. The thermal treatment was also performed to induce copper interdiffusion

throughout the samples in order to guarantee a better composition distribution of the alloy into the deposits, which, therefore, reflects also on the ensuing porosity. As mentioned before, the final nanoporous substrates were produced through an electrochemical de-alloying process. Indeed, it was observed in previous works (14) that nanoporous films can be obtained by selective electrochemical etching of the nobler component in a system where the more active component is passivated. Copper is thermodynamically more stable than Ni by 0.597 V, thus, its etching should be hindered in this particular binary system. However, the formation of a passive oxide film on Ni in sulfamate solutions allows the selective electrochemical etching of Cu (14). The electrochemical dealloying process was developed in the same solution used for the former deposition step, while a four-electrode cell was employed. The free-standing NiCu alloy foils were connected to the positive pole of the power generator, thus working as anode. The reference electrode was the saturated calomel, while two titanium nets were used as cathode, one in front and one behind the free-standing foils in order to guarantee a better Cu etching.

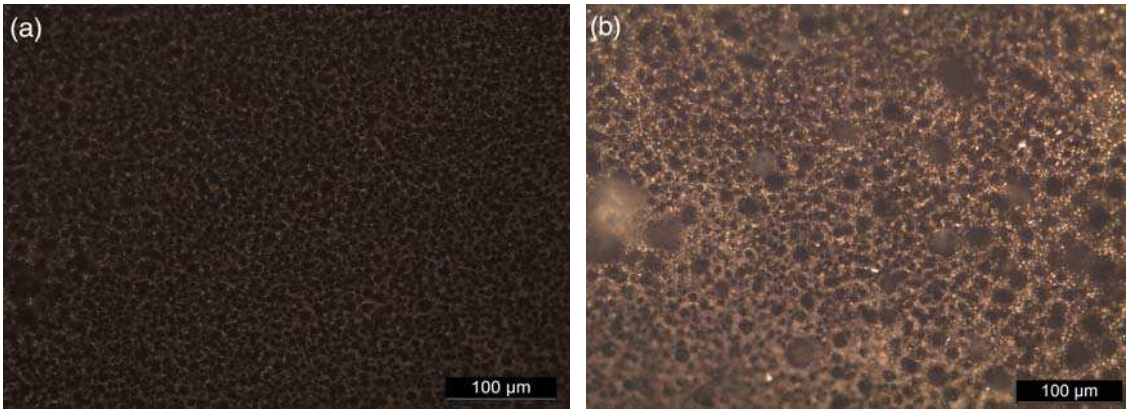

Figure 3. Optical images of free standing porous Ni foils with an initial copper content of 25 % (a) and 35 % (b).

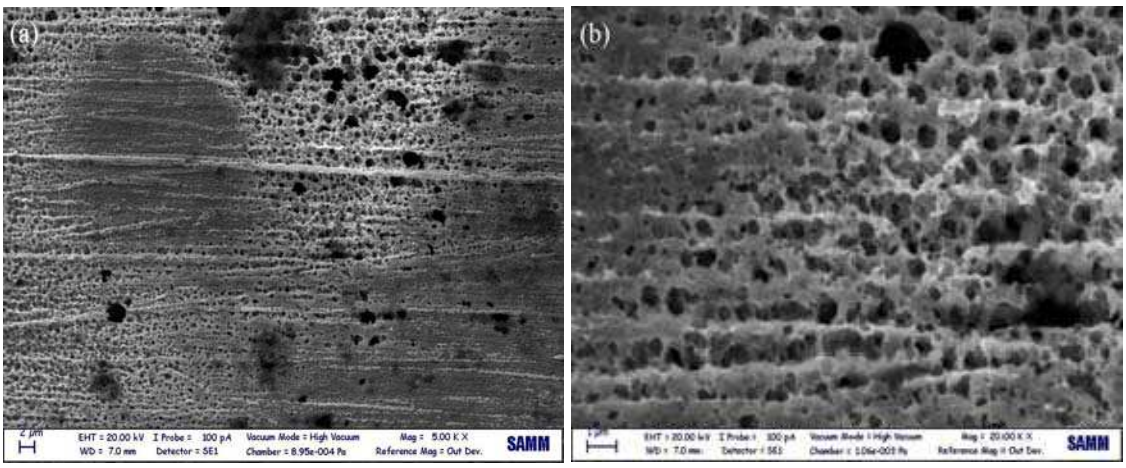

Figure 4. (a) and (b): SEM images of the free standing nanoporous Ni foil with initial
copper percentage of 20 %.

The experiments were carried out at room temperature, while the solution pH was raised till 8. Linear sweep voltammetry revealed that the best technique for copper etching is the

application of 15 cycles between 1.3 V and 1.6 V with a scan rate of 1 mV/s. It has not been possible to etch away all the Cu initially present in the samples. Indeed, a remaining 4 to 9% of Cu was still present in the final porous substrates and this was probably due to bulk copper strongly bound with nickel.
Furthermore, a significant difference between the initial and final samples thickness was noticed, meaning that during the de-alloying process a sort of collapse of the entire structure took place as a result of the nickel re-arrangement. Starting from deposits with an initial copper content in the range between 10 % and 40 %, free standing nanoporous Ni foils with different porosity were produced. In Fig.3 and Fig.4 optical and SEM images elucidate the characteristic morphology of the obtained samples. In particular, in Fig.3 is clear the influence of the initial copper content on the final porosity, as bigger pores were noticed when the initial Cu content was greater. Fig.4 clearly shows the presence of well-distributed nanopores into the etched samples. Pores of micrometric scale were also present, pointing that in those points a bigger content of Cu was present.
The obtained nanoporous Ni films were used as substrates for the graphene growth. Successful growths at 600 °C, 700 °C, and 800 °C were obtained, with lower graphene layers with increasing temperatures, as shown in the Raman spectra of Fig.5. Both the characteristic G and 2D peaks of graphene (15,16) were present in all three cases, approximately at 1580 cm^{-1} and 2660 cm^{-1}. However, the 2D peak was less intense compared to the G peak, indicating that the synthesized graphene was multi-layer and not single layer (15-17). In particular, as shown in the literature (15,16), for greater deposition temperatures (800 °C) the shape of the 2D peak is similar to the one of 4-5 layers graphene. Moreover, all the three samples showed a quite intense D peak due to the breathing mode of graphene (15,16) and characteristic of defected graphene structure. However, the presence of the D peak was expected since the NiCu substrates present a very defected and porous structure.

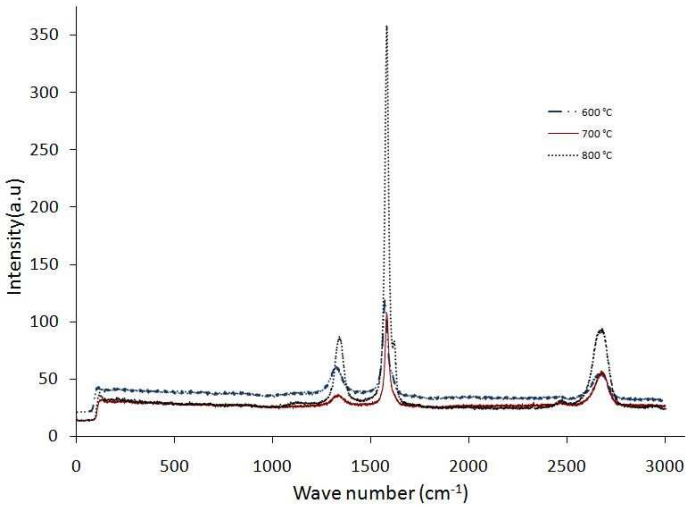

Figure 5. Raman spectra of CVD grown graphene on nanoporous Ni at different deposition temperatures.

In Fig.6, SEM images show the surface of the nanoporous Ni substrate prior and after graphene synthesis. From Fig.6 (b), the substrate appears wrapped in wrinkly graphene flakes (11,12). Wrinkles can form when two adjacent graphene flakes meet together during the cooling step. Indeed, large compressive stresses are incorporated into graphene

layers upon cooling, due to the negative coefficient of thermal expansion, which lead to layer buckling and stress relief by formation of wrinkles. These wrinkles probably form preferentially at grain boundaries or at boundaries between graphene domains with different thicknesses (11,12).

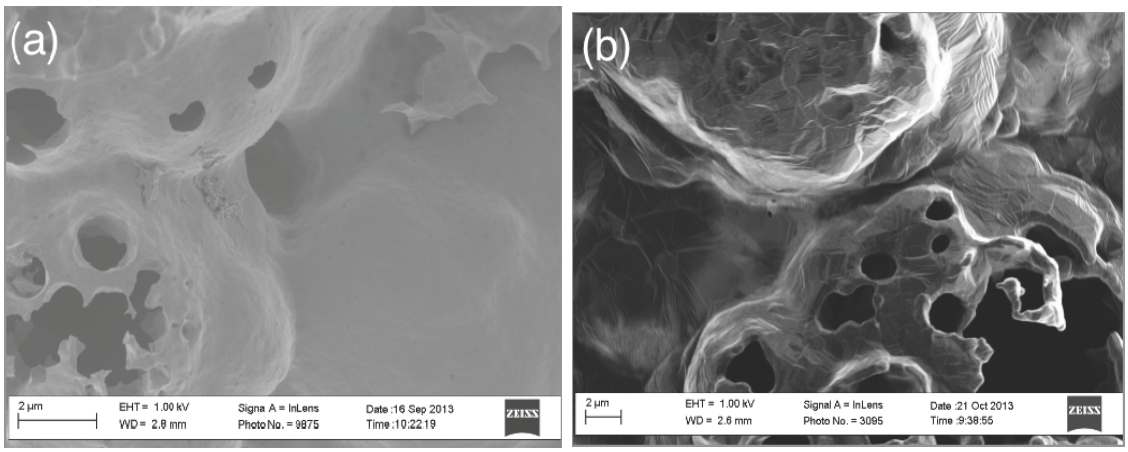

Figure 6. SEM images of the nanoporous Ni substrate surface prior (a) and after (b) graphene deposition.

Since the idea was to obtain a free-standing 3D nanoporous structure of graphene and to integrate it in MEMS for sensor application, a transferring process was necessary. The etching of the nanoporous Ni substrate was performed in a highly concentrated HCl solution and then the freestanding porous graphene was harvested with a piece of Si wafer, sonicated in isopropanol for 10 minutes and then washed with DI water. Subsequently, the whole system was let to dry on a heating plate at 80 °C in order to improve the adhesion between the Si wafer and graphene.
SEM images in Fig. 7 clearly show the 3D porous graphene structure. In particular, Fig. 7 exemplifies the three dimensional pores network indicating that the porosity of the Ni substrate was maintained also in the graphene structure. Furthermore, the presence of the characteristic graphene flakes separated by wrinkles is visible in the form of black lines on the structure.

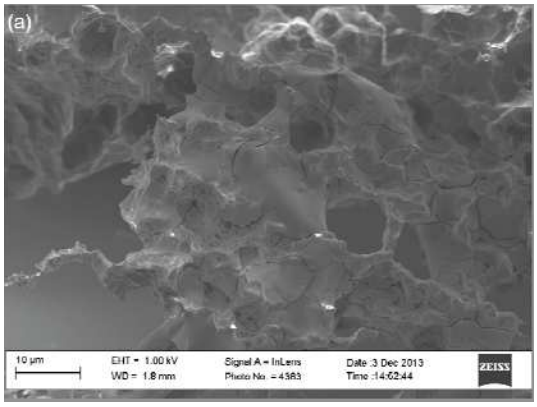

Figure 7. SEM images of the 3D nanoporous graphene structure transferred onto Si wafer.

Conclusions

A two-step process, via electroforming of NiCu and subsequent dealloying, yields a nanoporous Ni substrate. The chosen method is cost-effective, reliable, and reproducible, although the problem of residual copper present in the substrates after the etch step can influence the subsequent graphene growth. Therefore, further process refinement aimed to optimizing the electrochemical dealloying step would be desirable; such refinement may include leaving the samples in the etching solution for longer time and at lower applied potentials. Regardless, the successful synthesis of a three-dimensional nanoporous graphene structure on the electroplated Ni and its transfer to a silicon substrate demonstrate that 3D foam-like graphene films can be synthesized by highly scalable electrochemical methods and integrated with silicon. Subsequent functionalization of graphene, e.g., by nanoparticle decoration, can lead to the development of functional devices, such as gas sensors (18).

References

1. F. Traversi, V. Russo and R. Sordan, Appl. Phys. Lett., 94(22), 223312 (2009).
2. Y. M. Lin, A. Valdes-Garcia, S. J. Han, D. B. Farmer, I. Meric, Y. Sun, Y. Wu, C. Dimitrakopoulos, A. Grill, P. Avouris and K. A. Jenkins, Science, 332, 1294 (2011).
3. F. Schedin, A. K. Geim, S. V. Morozov, E. W. Hill, P. Blake, M. Katsnelson and K. S. Novoselov, Nat. Mater., 6(9), 652 (2007).
4. S. Zhu and T. Li, ACS Nano, 8(3), 2864 (2014).
5. M. D. Stoller, S. Park, Y. Zhu, J. An and R. S. Ruoff, Nano Lett., 8(10), 3498 (2008).
6. M. J. Allen, V. C. Tung and R. B. Kaner, Chem. Rev., 110, 132 (2010).
7. S. Benitez-Martinez and M. Valcarcel, Sens. Actuator B-Chem., 197, 350 (2014).
8. S. Pakapongpan, J. P. Mensing, D. Phokharatkul, T. Lomas and A. Tuantranont, Electrochim. Acta, 133, 294 (2014).
9. R. S. Edwards and K. S. Coleman, Durham University: Accounts of chemical research, 46(1), 23 (2012).
10. W. Chen, Z. Fan, G. Zeng and Z. Lai, J. Power Sources, 225, 251 (2013).
11. S.J. Chae, F. Gunes, K. Kim, E. S. Kim, G. H. Han, S. M. Kim, H. Shin and S. Yoon, Adv. Mater., 21, 2328 (2009).
12. Z. Li, P. Wu, C. Wang, X. Fan, W. Zhang, X. Zhai, Z. Li, J. Yang and J. Hou, Low-Temperature growth of graphene by chemical vapor deposition using solid and liquid carbon sources, ACS Nano, University of Science and Technology of China (2011).
13. P. Calleja, et al., Electrochim. Acta, 62, 381 (2012).
14. L. Sun, C. Chien and P. Searson, Chem. Mater., 16, 3125 (2004).
15. A. C. Ferrari, Solid State Commun., 143, 47 (2007).
16. A. C. Ferrari and D.M. Basko, Raman spectroscopy as a versatile tool for studying the properties of graphene, Cambridge Graphene Centre, Cambridge University, Cambridge, UK (2013).
17. A. Jorio, R. Salta, G. and M. Dresselhaus, Raman spectroscopy in graphene related systems, Wiley-VCH Verlag GmbH & Co., Germany (2011).
18. A. Gutes, B. Hsia, A. Sussman, W. Mickelson, A. Zettl, C. Carraro, R. Maboudian, Nanoscale, 4, 438 (2012).